A reversible solvent segregation transition at grain boundaries in gold-platinum alloys

Sebastian Calderon[1], Wen-Yu Chen[1], Md. Shariful Islam[2], Sai S. Tripathy[1], Maarten P. de Boer[2], Elizabeth C. Dickey[1], and Gregory S. Rohrer[1]

[1]Department of Materials Science and Engineering

[2]Department of Mechanical Engineering

Carnegie Mellon University, Pittsburgh, PA, 15213

July 1 2025

Abstract

Solute segregation to grain boundaries in polycrystalline metals and ceramics is a well-known phenomenon that reduces the total energy of the material. In this letter, the segregation of the solvent (Au) to grain boundaries in a binary $Au_{1-x}Pt_x$ (x = 0.15 to 0.18) alloy is demonstrated. After heating in the range of 500 °C to 600 °C and quenching to room temperature, grain boundaries in the alloy are enriched in Au at a mean level of ~ 4 atoms/nm^2. When the alloy is annealed at 300 °C and quenched, the mean grain boundary composition is closer to the bulk composition. When the alloy is reheated to 500 °C, the segregation is reestablished, demonstrating that the transformation from the strongly segregated complexion to the weakly segregated complexion is reversible. The driving force for the solvent segregation is likely the lower grain boundary energy of Au in comparison to Pt.

The chemical compositions of grain boundaries in polycrystals of multicomponent materials usually differ from the bulk, a phenomenon known as grain boundary segregation [1]. Grain boundary segregation often alters materials properties with a wide variety of possible outcomes, depending on the material. For example, the segregation of Ga to grain boundaries in Mg increases the ductility of the alloy [2] while the segregation of Bi to grain boundaries in Ni makes the alloy more brittle [3]. Grain boundary segregation is thought to stabilize nanocrystalline structures [4] and improve the strength of Ni-base alloys [5].

The composition of a grain boundary in an alloy, determined by segregation, is one characteristic of the grain boundary complexion, sometimes called the grain boundary phase [6, 7]. Controlling the grain boundary complexion is viewed as a tool to control the properties of polycrystalline materials [8, 9]. In all prior observations of grain boundary segregation in binary alloys, it is the minority component of the alloy (solute) that segregates to the grain boundary [1]. This is because the partitioning of the solute in the grain boundary typically reduces the free energy of the material by reducing the grain boundary energy. However, it is also possible that solvent enrichment reduces the grain boundary energy. In the past, this phenomenon has been described as antisegregation and while not documented experimentally, has been predicted by simulations [10]. Here it is referred to as "solvent segregation" as this term is more descriptive and the natural opposite of solute segregation.

Udler and Seidman [11] simulated segregation to a grain boundary in a dilute Au-Pt alloy and predicted that the solvent, Au, would segregate. Murdoch and Schuh [12] used a Miedema-type model to estimate segregation enthalpies for about 2500 binary alloys and found that ≈ 1/5 of the total, including Au-rich alloys containing Pt, were expected to exhibit solvent segregation. More recently, density functional theory calculations of Au-Pt alloys by Yao et al. [13] also predicted the segregation of Au in Au-rich Au-Pt alloys. While grain boundary segregation in Pt rich Au-Pt alloys is well studied and Au (the solute) is known to segregate [14-17], grain boundary segregation in Au-rich alloys has not been studied experimentally. Here we describe solvent (Au) segregation to grain boundaries in a $Au_{1-x}Pt_x$ ($x = 0.15$ to 0.18) alloy after heating in the range of 500 °C to 600 °C. A distinct grain boundary complexion, with negligible segregation, results from heating the alloy at 300 °C. The experiments described here demonstrate that there is a reversible transition between the strongly segregated and weakly segregated complexions.

50 nm thick $Au_{1-x}Pt_x$ thin films were co-sputtered onto rotating substrates at room temperature from angled Au and Pt targets in a Kurt Lesker Pro Line PVD75 DC Magnetron Co-Sputtering deposition system with a base pressure of 5×10^{-8} torr. To achieve the desired composition, the growth rate as a function of power was calibrated for each target. The films were deposited on 10 nm thick silicon nitride membranes supplied by Norcada and thermal E-chip devices with 40 nm thick silicon nitride membranes (E-FHDS-VO) from Protochips for *ex-situ* and *in-situ* experiments, respectively. For the *in situ* experiment, the film was sputtered through a shadow mask, so that the film did not create a continuous electrical path that could short the circuit. Energy dispersive X-ray spectroscopy (EDS) conducted in the scanning transmission electron microscope (STEM) indicated that the Pt compositions of the films deposited without the shadow mask corresponded to $x = 0.15$ and those with the mask were $x = 0.18$. This difference is thought to result from the geometry of the shadow mask and the metal sources, inadvertently allowing less Au through the aperture in the mask compared the blanket films where there was no mask.

The portion of the Au-Pt phase diagram relevant to the current studies is shown in Fig. 1(A), with the position of the phase boundary consistent with the results of Xu et al. [18]. The samples were initially heated in air to 500 °C for 2 h. This led to the microstructure illustrated in Fig. 1(B), which has an average grain size of 125 nm and no sign of dewetting. Because the grain size is more than twice the film thickness, the majority of the grains extend through the thickness of the film. Diffraction patterns (see Fig. S1) indicate that the material is single phase with the structure of the fcc Au solid solution (at these temperatures and compositions, the phase diagram indicates that the Pt-rich solid solution should make up as much as 7 % of the film). Films heated at 300 °C and 400 °C for 2 h were also single phase. These observations suggest that there is a kinetic limitation in this nanocrystalline film that suppresses the nucleation of the Pt-rich phase in the time scale of this experiment, the position of the phase boundary is incorrect, or there is a systematic error in the EDS quantification.

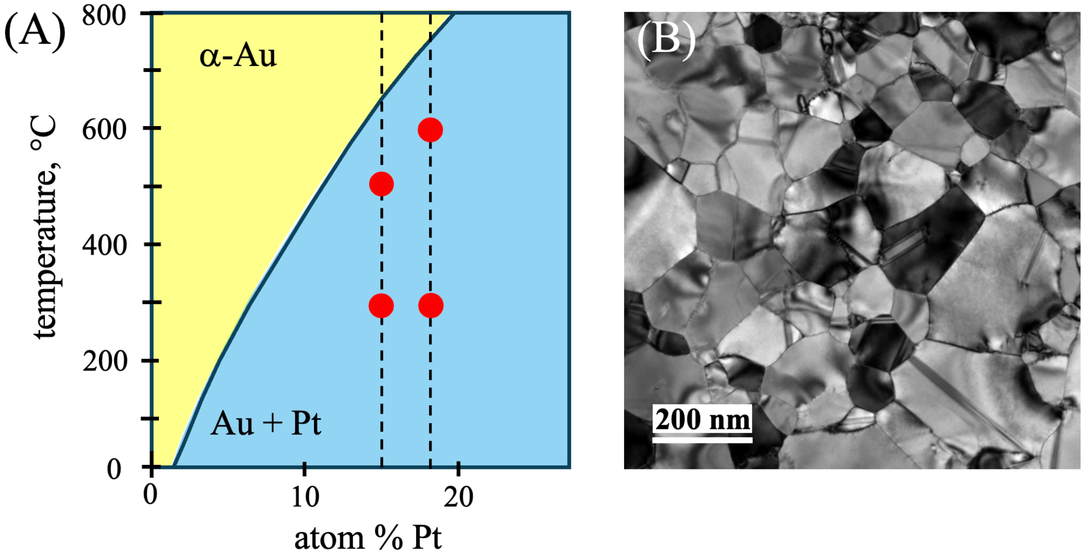

Figure 1. Composition and microstructure of the Au-Pt films. (A) Portion of the Au-Pt binary phase diagram [18]. The locations of the annealing experiments are marked with red circles. (B) Bright field TEM image of a $Au_{0.85}Pt_{0.15}$ thin film heated for 2 h at 500 °C.

To evaluate the local compositional variation, STEM images and EDS elemental maps were recorded in a Thermo Fisher Themis 200 G3 aberration-corrected STEM operated at 200 kV. Data were collected with a high angle annular dark-field (HAADF) detector, a probe convergence angle of 17 mrad, and a camera length that results in acceptance angles from 70 to 200 mrad. Note that under these imaging conditions, the HAADF images are dominated by diffraction contrast (as very little compositional contrast is expected between Au and Pt). Iterative elemental maps of 512 x 512 pixels are acquired with a dwell time per pixel of 10 µs at 200 keV over 360 frames using a Super-X EDS detector. The total electron screen current was 1 nA, resulting in a total dose per frame of the order of 10^8 $e^-/Å^2$. Elemental maps are plotted using the ratio between the Au and Pt L_α X-ray emission line intensities after background subtraction. The Pt grain boundary excess (Γ_{Pt}) was calculated according to [19, 20]:

$$\Gamma_{Pt} = NW\left[\left(\frac{c_{Pt}}{c_{Au}}\right)^{gb} - \left(\frac{c_{Pt}}{c_{Au}}\right)^{bulk}\right] \qquad (1),$$

where N is the gold density in atoms/nm^3 and W is the width of the grain boundary analyzed (~ 4 nm). The bulk Pt and Au concentration ratio $\left(\frac{c_{Pt}}{c_{Au}}\right)^{bulk}$ is calculated as the average of $\frac{c_{Pt}}{c_{Au}}$ in the two neighboring grains (see supplementary information for more details).

A HAADF image and corresponding composition map of the sample after annealing at 500 °C for 2 h in air are presented in Fig. 2A and 2B. The composition map in Fig. 2B shows linear features with enhanced Au concentrations relative to the bulk. A close comparison with the image in Fig. 2A shows that the positions of the lines correlate with grain boundaries. Tests to determine if the beam exposure influenced the segregation (See Fig. S3) indicated that the Au concentrations were constant with time. There are also some grain boundaries where no segregation is evident. Low energy grain boundaries are expected to resist segregation, so this is not unexpected [21-24]. For example, one of the grains in Fig. 2A is bisected by a very straight boundary that, based on its morphology, is likely a twin boundary (see arrow). Twins have the minimum grain boundary energy in Au [25] and no segregation is detected at this boundary. The small black features in the HAADF images have been identified as pores (see Fig. S4).

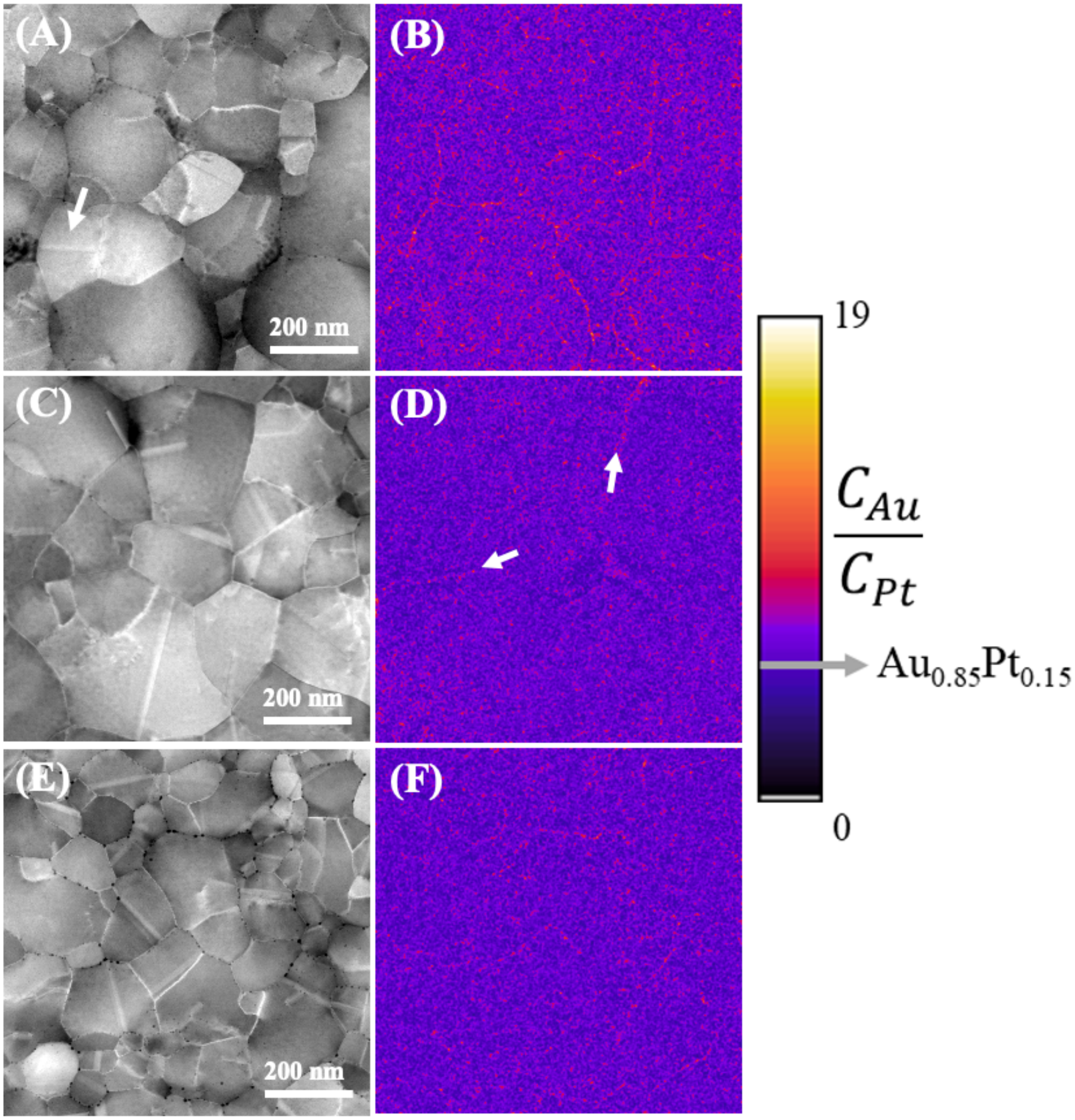

Figure 2. Microstructure images (HAADF) and composition maps (EDS data) of $Au_{0.85}Pt_{0.15}$ thin films. (A&B) Film annealed at 500 °C for 2 h. (C&D) The same film after annealing at 300 °C for 2 h. (E&F) The same film after annealing at 500 °C for 1 h.

After analyzing the film annealed at 500 °C, it was annealed at 300 °C for 2 h in air and quenched to room temperature. A similar (but not identical) area of the film was examined and the results are presented in Fig. 2(C&D). While there are a few locations that appear to have elevated Au concentrations along lines (see arrows), the composition appears to be more uniform than what was found after the 500 °C anneal. To assess reversibility following these analyses, the sample was heated for 1 h at 500 °C in air, and another area was examined and the results are shown in Fig. 2(E&F). The composition map in Fig. 2F again shows enhanced Au concentrations along lines correlated to a subset of the grain boundaries. These results suggest that there is a reversible transition between a grain boundary complexion at 500 °C, where a majority of the grain boundaries have an enhanced Au (solvent) concentration and 300 °C where the majority of the grain boundaries have concentrations that are nearly equivalent to the bulk.

While it seems clear that there is enhanced Au segregation to the grain boundaries in $Au_{0.85}Pt_{0.15}$ at 500 °C, it is also clear that it is not uniform. To quantify the mean amount of segregation and the variation, the compositions of at least 40 individual grain boundaries were measured and the results are summarized in Fig. 3. The ratio of the Pt and Au concentration (C_{Pt}/C_{Au}) was measured within a well-defined area, at every grain boundary in the image, and from an identical area in the adjacent grains. The Pt excess at the grain boundary was then calculated using Eq. 1. Histograms of the Pt grain boundary excess are shown in Fig. 3A for the three different annealing conditions and the same data are represented using a box and whisker plot in Fig. 3B. The data clearly show a negative excess of Pt in the grain boundaries after annealing at 500 °C; the negative Pt excess reflects an excess of Au, which we refer to as solvent segregation. On the other hand, the Pt excess of the grain boundaries after annealing at 300 °C is close to zero, indicating limited segregation. The results show that the transition from the strongly segregated state to the weakly segregated state is reversible.

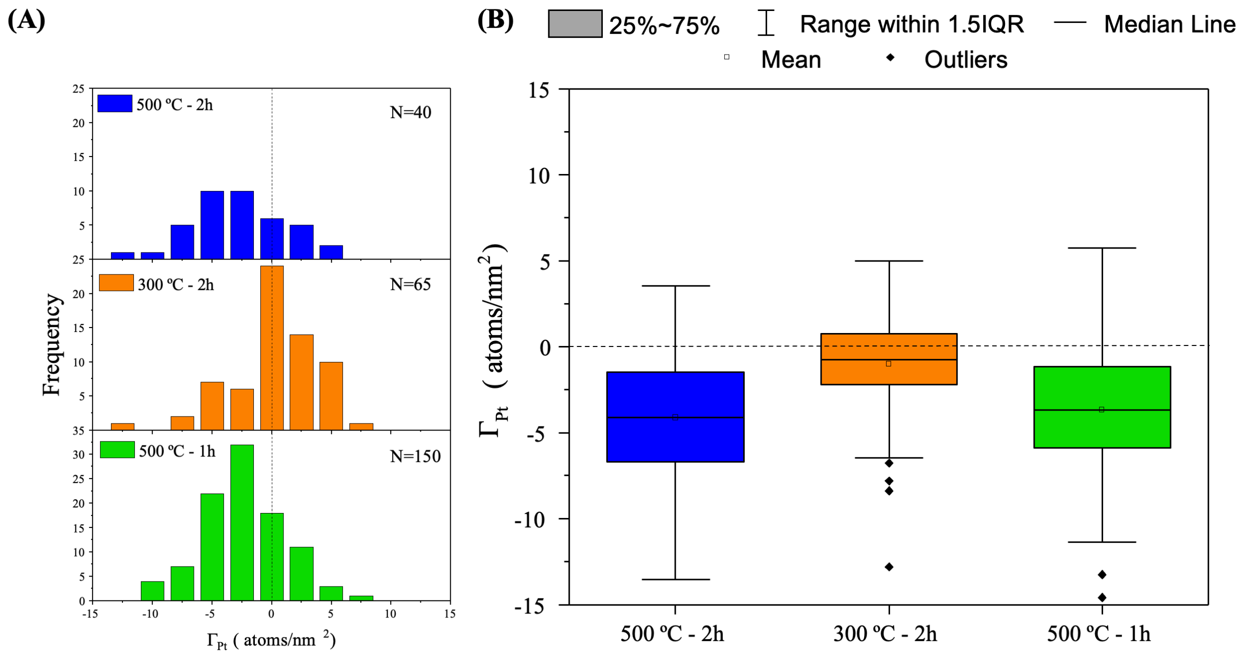

Figure 3. Pt grain boundary excess at grain boundaries in Au$_{0.85}$Pt$_{0.15}$ after different annealing conditions. (A) Histogram of Pt excess after a 2 h anneal at 500 °C (top), after a 2 h anneal at 300 °C (middle) and after a 1 h anneal at 500 °C (bottom). (B) Box and whisker plot of the distributions. The line is the median, the boxes are the nearest two quartiles of data, the bars indicate the other two quartiles, and the dots are outliers.

We attempted a fully *in situ* heating experiment to track the composition of individual grain boundaries. However, rapid sublimation of the sample into the microscope's dynamic vacuum [26] made this impossible. Quantitative estimates of the sublimation rate are provided in the supplemental information (see Fig. S5). It was possible, however, to conduct the following partially *in situ* measurement in which the Au$_{0.82}$Pt$_{0.18}$ sample deposited on the heating chip was initially annealed in air outside of the microscope (to reduce sublimation) at 600 °C and air quenched. The 600 °C anneal was used so that grain growth would not occur during subsequent anneals at lower temperature. Subsequent heat treatments at or above 500˚C were also carried out in air, while heat treatments at 300˚C could be carried out inside the microscope vacuum, assuming the estimated sublimation rate of 2×10^{-5} monolayers/min at 300 °C (see Fig. S5) is correct.

As demonstrated in Fig. 4B, excess Au is found at a subset of the grain boundaries for the sample annealed at 600 °C, consistent with what was observed for the sample heated *ex situ* at 500 °C. To facilitate examination of the exact same population of grain boundaries, the sample was then heated at 300 °C for 2 h while still in the microscope. As in the *ex situ* experiment, the localized concentration of Au at the grain boundaries decreases to nearly the same as the bulk Au concentration except for a few examples, (see Fig. 4D). After heating the sample to 575 °C for 0.5 h in air, again to prevent sublimation, and returning it to the microscope, the Au concentration at the grain boundaries is found to increase. It is mostly the same grain boundaries that concentrate Au during the first 600˚C anneal (Fig. 4B) that also concentrate gold during the second 575˚C anneal (Fig. 4F), demonstrating the reversibility of the complexion transition.

Note that after the 300 °C anneal in the microscope, some Pt-rich regions develop (see dashed arrows in Figs. 4C and 4D). These regions are precipitates of the Pt rich phase. Because they were not found in any of the *ex situ* experiments, it is assumed that sublimation of Au in the microscope at 300 °C was larger than estimated and further enriched these areas in Pt and promoted phase separation. Nevertheless, the same reversible transformation of the grain boundary compositions was observed.

The distribution of boundary compositions in this experiment (analogous to Fig. 3) are presented in Fig. S6. To illustrate the reversibility of the transition at a single grain boundary, the composition of the grain boundary labeled with the double headed white arrow in Figs. 4A, 4C and 4E was quantified at the three temperatures. Line profiles of the C_{Au}/C_{Pt} ratio were averaged in this region following the three anneals, and these profiles are illustrated in Fig. 5. The solvent segregation maximizes at the grain boundary after the anneals at 600 °C and 575 °C, but the segregation is very weak after the 300 °C anneal.

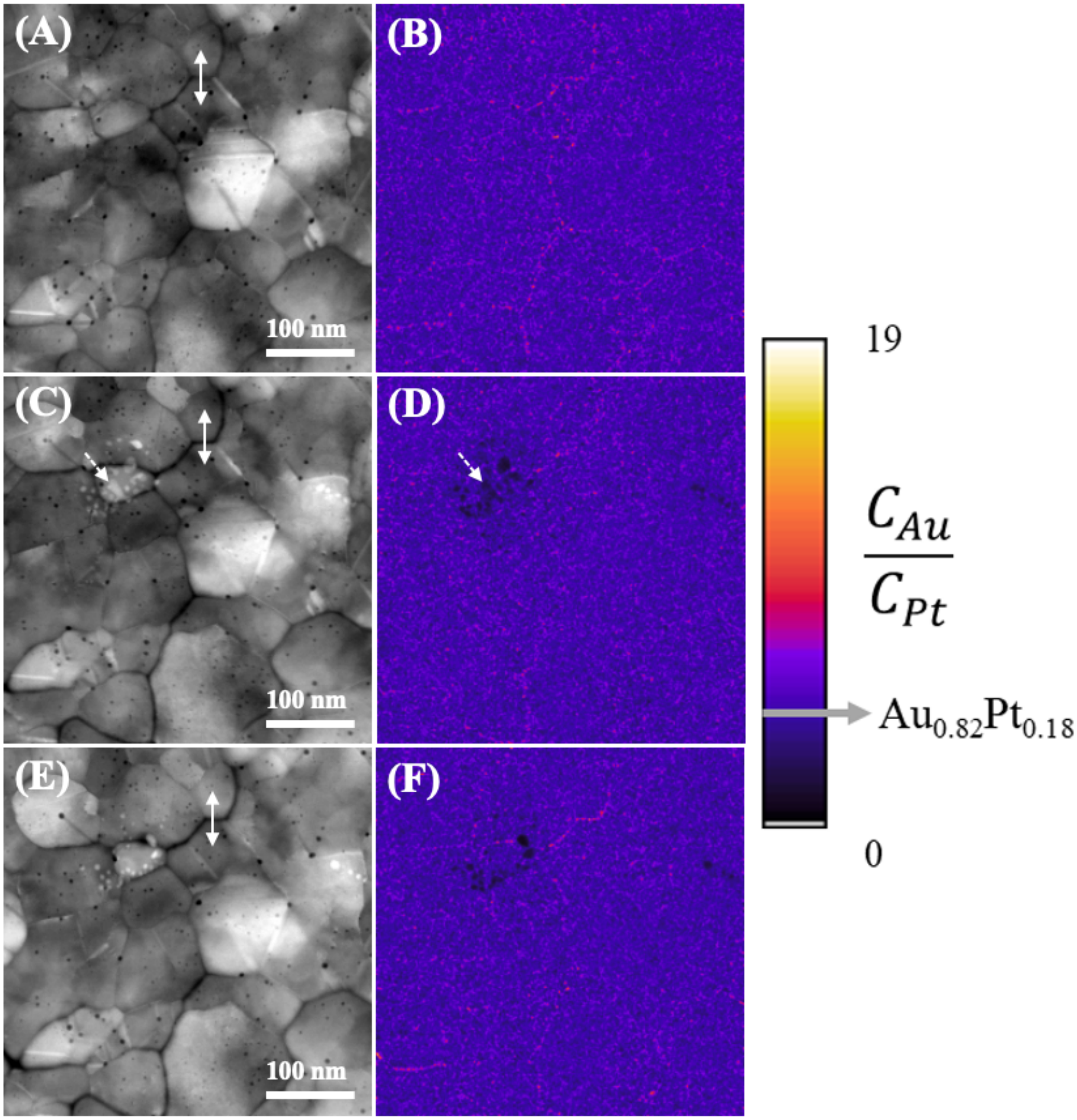

Figure 4. Microstructure images (HAADF) and composition maps (EDS data) of $Au_{0.82}Pt_{0.18}$ thin films. (A&B) Film annealed at 600 °C for 2 h. (C&D) The same film after annealing at 300

°C for 2 h. (E&F) The same film after annealing at 575 °C for 0.5 h. The white double headed arrows in A, C, and E mark the boundary whose composition is illustrated in Fig. 5.

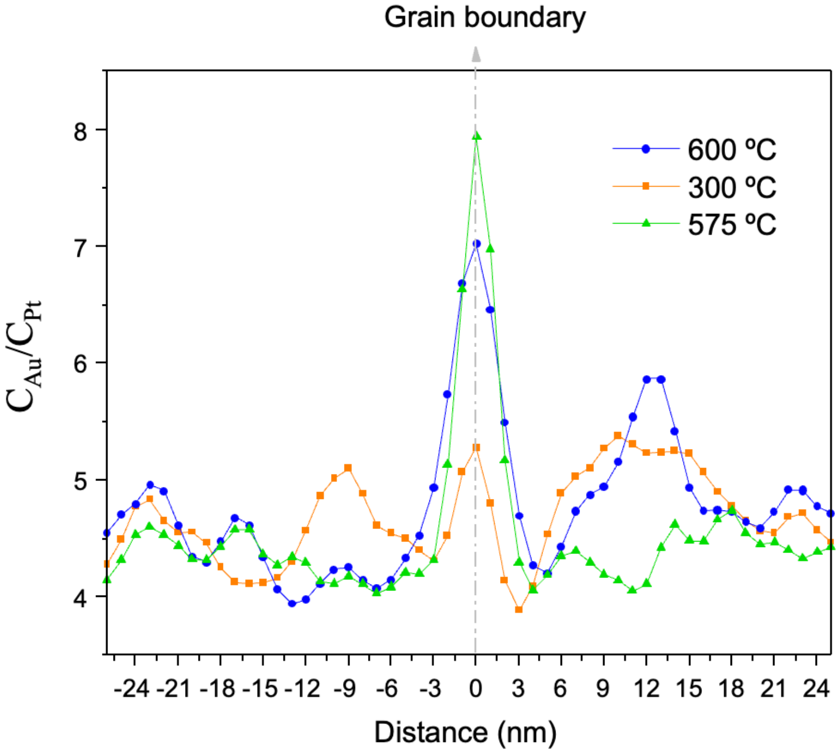

Figure 5. Composition changes at a single boundary in the $Au_{0.82}Pt_{0.18}$ sample with different heat treatments. Composition of the grain boundary at the 600 °C, 300 °C, and 575 °C at the position of the white arrows in Fig. 4A, 4C, and 4E.

The results clearly show that at temperatures between 500 °C and 600 °C, the solvent (Au) segregates to grain boundaries in $Au_{1-x}Pt_x$. Gold segregation was predicted by computer simulations [11], empirical models [12], and DFT calculations [13], but was not previously observed. Furthermore, there are no known experimental reports of solvent segregation in any binary alloy. This is despite predictions by Murdoch and Schuh [12] that ≈ 1/5 of all binary alloys should show solvent segregation. We recognize that segregation sites at grain boundaries have a spectrum of segregation enthalpies and that some sites prefer solvent atoms and others prefer solute atoms [27]. A recent calculation of the spectrum of segregation enthalpies in Au-Pt reports that the mean segregation enthalpy is 8 kJ/mol and the standard deviation is 13 kJ/mol, meaning that the majority of sites promote solvent segregation [28]. This agrees with the prior work predicting solvent segregation [11-13]. We should also mention that there are some well-documented examples of solute concentrations in grain boundaries falling below the solvent concentration in ternary and more complex alloys, but this is the result of a third strongly segregating component excluding the solute from the grain boundary [1]. A well-documented example occurs in ternary Fe-Si-P alloys where Si and P are the dilute components. In the ternary alloy, P strongly segregates and excludes Si from the boundaries [29]. However, in the binary Fe-Si alloy, Si segregates to the boundaries [30].

There are a variety of factors that contribute to the segregation enthalpy and promote solvent segregation. The most important factors are the interaction energy between Au and Pt, their size difference (which contributes to the elastic energy), and the grain boundary energy. Au and Pt are immiscible and do not form binary compounds [18, 31], implying that they greatly favor Au-Au and Pt-Pt bonds compared to Au-Pt bonds. Au and Pt differ by only one atomic number and their sizes differ by only 4 %, so the elastic contribution is small. On the other hand, the surface and grain boundary energies of Au and Pt are significantly different. Surface energies are closely related to grain boundary energies [32]; the experimentally determined surface energies of Au and Pt are 1.14 J/m^2 and 1.71 J/m^2, respectively, at their melting points [33]. Selected grain boundary energies calculated at 0 K for Au are less than half of those for Pt [13]. The lower grain boundary energy in Au means that Au-rich grain boundaries are energetically preferred over Pt-rich boundaries, even at the cost of sustaining Au-Pt bonds in the bulk.

Using the McLean isotherm [34] for grain boundary adsorption and the computed mean segregation enthalpy (8 kJ/mol [28]), we can compute the expected grain boundary composition (see Fig. S7). This simple model predicts that the ratio of Au to Pt in the boundary is about 16 at

500 °C; the boundary in Fig. 5 has a ratio of 7 to 8. Note that the different segregation to each boundary makes quantitative comparisons difficult, but the simple prediction assuming a segregation enthalpy of 8 kJ/mol over-estimates the observed amount of segregation at the average grain boundary. The simple models also predict an increase in enrichment at lower temperature, but this is not what is observed. This is because of the complexion transition [7]. An increase in the concentration of segregant cannot be predicted by the McLean isotherm [34] because it does not account for multilayer absorption or interactions between adsorbates. More advanced models [35-38] predict that when the interactions between segregating atoms is strong, there can be first order transitions that increase the concentration of the segregating atoms at the interface. That is consistent with what is observed here.

The results presented here also provide the first direct evidence that a complexion transition involving a composition change is reversible. The reversibility of grain boundary faceting transitions that do not involve changes in composition has been documented [39]. Previously, the only experimental report of the reversibility of a transition involving a composition change was indirect, through the observation of grain boundary thermal grooves from microstructures with different grain sizes [40]. The transition from solvent segregation to no segregation and back occurs on a time scale on the order of 30 to 120 minutes, presumably limited only by the time for atomic diffusion. The bulk self-diffusion coefficient of Au at 300 °C is 3×10^{-17} cm^2/s and at 500 °C is 2.3×10^{-13} cm^2/s [41]. This leads to diffusion distances of 11 nm (300 °C) and 1000 nm (500 °C). The distance at 500 °C is greater than the grain size, so transport is not a problem. The distance at 300 °C, while much smaller than the grain size, is likely sufficient, even without short circuit diffusion on the surface [42]; these alloys contain more than 48 Au atoms/nm^3, so the surface excess (4 Au /nm^3) could be sourced from a thin region near the grain boundary. This is another interesting difference between solvent and solute segregation, because longer range diffusion might be required to equilibrate solute distributions in dilute alloys.

It is recognized that the grain boundary complexion transition described here encompasses most, but not all, grain boundaries. Between 500 °C and 600 °C, not all grain boundaries have Au enrichment. Likewise, at 300 °C, there is no detectible segregation to most, but not all, grain boundaries. This is consistent with past theories [43] and experiments on complexion transitions [23]. It has been concluded that at any given temperature, it is the highest energy grain boundaries (those where the greatest amount of energy can be eliminated) that are most likely to transform. Therefore, those that retain some Au segregation at 300 °C are expected to be the highest energy grain boundaries and those that remain unsegregated at the highest temperatures are expected to be the lowest energy grain boundaries. According to recent calculations [13], grain boundary energies in Au vary from a minimum of 0.004 J/m^2 (60°/[111]|(111)) to 0.415 J/m^2 (36°/[100]|(310)), which can plausibly account for the observed differences.

In summary, compositional mapping of $Au_{1-x}Pt_x$ ($0.15 \leq x \leq 0.18$) thin films after annealing at ≥ 500 °C demonstrates solvent segregation – the enrichment of Au at the grain boundaries. This is opposite to the commonly observed phenomenon of solute segregation. While this has not previously been documented, it might be common in alloys of metals with very different grain boundary energies and provide a potential new avenue for grain boundary engineering. The strongly solvent segregated complexion can transform to a weakly segregated complexion by annealing at 300 °C. The transition between these two states is reversible and has been observed *ex-situ* by heating in air and *in situ* by heating in the microscope.

Acknowledgement

We acknowledge the support of the Department of Energy through Grant DOE BES **DE-SC0023231**. The authors also acknowledge use of the Materials Characterization Facility at Carnegie Mellon University supported by grant MCF-677785.

Declaration of competing interest

The author Gregory S. Rohrer is Coordinating Editor for Scripta Materialia and was not involved in the editorial review or the decision to publish this article.

Author Contributions

Sebastian Calderon: Investigation, Visualization, Reviewing and Editing. Wen-Yu Chen: Investigation, Visualization, Reviewing and Editing. Md. Shariful Islam: Investigation, Reviewing and Editing. Sai S. Tripathy: Investigation, Reviewing and Editing. Maarten P. de Boer: Obtaining Funding, Supervision, Conceptualization, Methods, Reviewing, and Editing. Elizabeth C. Dickey: Supervision, Conceptualization, Methods, Reviewing, and Editing. Gregory S. Rohrer: Supervision, Conceptualization, Methods, Writing, Reviewing, and Editing.

References Cited

[1] P. Lejcek. Grain Boundary Segregation in Metals. 1 ed., Springer Berlin, Heidelberg, Heidelberg, 2010, https://doi.org/10.1007/978-3-642-12505-8.

[2] X.Y. Zhou, P. Mathews, B. Berkels, W. Delis, S. Saood, A.S.A. Alhassan, P. Keuter, J.M. Schneider, S. Korte-Kerzel, S. Sandlöbes-Haut, D. Raabe, J. Neugebauer, G. Dehm, T. Hickel, C. Scheu, S.Y. Zhang. Materials Design by Constructing Phase Diagrams for Defects, Adv. Mater. (2024), http://dx.doi.org/10.1002/adma.202402191.

[3] J. Luo, H.K. Cheng, K.M. Asl, C.J. Kiely, M.P. Harmer. The Role of a Bilayer Interfacial Phase on Liquid Metal Embrittlement, Science 333 (2011) 1730-1733, http://dx.doi.org/10.1126/science.1208774.

[4] T. Chookajorn, H.A. Murdoch, C.A. Schuh. Design of Stable Nanocrystalline Alloys, Science 337 (2012) 951-954, http://dx.doi.org/10.1126/science.1224737.

[5] D. Raabe, M. Herbig, S. Sandlöbes, Y. Li, D. Tytko, M. Kuzmina, D. Ponge, P.P. Choi. Grain boundary segregation engineering in metallic alloys: A pathway to the design of interfaces, Curr. Opin. Solid State Mater. Sci. 18 (2014) 253-261, http://dx.doi.org/10.1016/j.cossms.2014.06.002.

[6] P.R. Cantwell, T. Frolov, T.J. Rupert, A.R. Krause, C.J. Marvel, G.S. Rohrer, J.M. Rickman, M.P. Harmer. Grain Boundary Complexion Transitions. in: Clarke DR, (Ed.). Ann. Rev. Mater. Res., vol. 50. 2020. pp. 465-492, http://dx.doi.org/10.1146/annurev-matsci-081619114055.
[7] P.R. Cantwell, M. Tang, S.J. Dillon, J. Luo, G.S. Rohrer, M.P. Harmer. Grain boundary complexions, Acta Mater. 62 (2014) 1-48, http://dx.doi.org/10.1016/j.actamat.2013.07.037.
[8] V. Devulapalli, E.Z. Chen, T. Brink, T. Frolov, C.H. Liebscher. Topological grain boundary segregation transitions, Science 386 (2024) 420-424, http://dx.doi.org/10.1126/science.adq4147.
[9] S. Korte-Kerzel, T. Hickel, L. Huber, D. Raabe, S. Sandlöbes-Haut, M. Todorova, J. Neugebauer. Defect phases - thermodynamics and impact on material properties, Int. Mater. Rev. 67 (2022) 89-117, http://dx.doi.org/10.1080/09506608.2021.1930734.
[10] S.M. Foiles. Calculation of grain-boundary segregation in Ni-Cu alloys, Phys. Rev. B 40 (1989) 11502-11506, http://dx.doi.org/10.1103/PhysRevB.40.11502.
[11] D. Udler, D.N. Seidman. Solute segregation at [001] tilt boundaries in dilute FCC alloys, Acta Mater. 46 (1998) 1221-1233, http://dx.doi.org/10.1016/S1359-6454(97)00297-8.
[12] H.A. Murdoch, C.A. Schuh. Estimation of grain boundary segregation enthalpy and its role in stable nanocrystalline alloy design, J. Mater. Res. 28 (2013) 2154-2163, http://dx.doi.org/10.1557/jmr.2013.211.
[13] X. Yao, Y.F. Guo, W. Li, K. Kokko, C.L. Li, L. Vitos. First-principles study on segregation anisotropy of grain boundaries in Pt-Au alloys, J. Appl. Phys. 137 (2025), http://dx.doi.org/10.1063/5.0238622.
[14] F. Abdeljawad, P. Lu, N. Argibay, B.G. Clark, B.L. Boyce, S.M. Foiles. Grain boundary segregation in immiscible nanocrystalline alloys, Acta Mater. 126 (2017) 528-539, http://dx.doi.org/10.1016/j.actamat.2016.12.036.
[15] C.M. Barr, S.M. Foiles, M. Alkayyali, Y. Mahmood, P.M. Price, D.P. Adams, B.L. Boyce, F. Abdeljawad, K. Hattar. The role of grain boundary character in solute segregation and thermal stability of nanocrystalline Pt-Au, Nanoscale 13 (2021) 3552-3563, http://dx.doi.org/10.1039/d0nr07180c.
[16] P. Lu, F. Abdeljawad, M. Rodriguez, M. Chandross, D.P. Adams, B.L. Boyce, B.G. Clark, N. Argibay. On the thermal stability and grain boundary segregation in nanocrystalline PtAu alloys, Materialia 6 (2019), http://dx.doi.org/10.1016/j.mtla.2019.100298.
[17] J.M. Monti, E.M. Hopkins, K. Hattar, F. Abdeljawad, B.L. Boyce, R. Dingreville. Stability of immiscible nanocrystalline alloys in compositional and thermal fields, Acta Mater. 226 (2022), http://dx.doi.org/10.1016/j.actamat.2022.117620.
[18] X.N. Xu, Y.P. Ren, C.F. Li, S. Li, G.W. Qin. Thermodynamic assessment of Au-Pt system, T. Nonferr. Metal. Soc. 22 (2012) 1432-1436, http://dx.doi.org/10.1016/S1003-6326(11)61337-X.
[19] J.A.S. Ikeda, Y.M. Chiang, A.J. Garrattreed, J.B. Vandersande. Space-charge segregation at grain-boundaries in titanium dioxide. 2. Model experiments, J. Am. Ceram. Soc. 76 (1993) 2447-2459, http://dx.doi.org/10.1111/j.1151-2916.1993.tb03965.x.
[20] Q.L. Wang, G. Lian, E.C. Dickey. Grain boundary segregation in yttrium-doped polycrystalline TiO_2, Acta Mater. 52 (2004) 809-820, http://dx.doi.org/10.1016/j.actamat.2003.10.016.
[21] M. Tang, W.C. Carter, R.M. Cannon. Diffuse interface model for structural transitions of grain boundaries, Phys. Rev. B 73 (2006) 14, http://dx.doi.org/10.1103/PhysRevB.73.024102.

[22] M. Tang, W.C. Carter, R.M. Cannon. Grain boundary transitions in binary alloys, Phys. Rev. Lett. 97 (2006) 4, http://dx.doi.org/10.1103/PhysRevLett.97.075502.

[23] S.A. Bojarski, M.P. Harmer, G.S. Rohrer. Influence of grain boundary energy on the nucleation of complexion transitions, Scripta Mater. 88 (2014) 1-4, http://dx.doi.org/10.1016/j.scriptamat.2014.06.016.

[24] G.S. Rohrer. The role of grain boundary energy in grain boundary complexion transitions, Curr. Opin. Solid State Mater. Sci. 20 (2016) 231-239, http://dx.doi.org/10.1016/j.cossms.2016.03.001.

[25] E.A. Holm, D.L. Olmsted, S.M. Foiles. Comparing grain boundary energies in face-centered cubic metals: Al, Au, Cu and Ni, Scripta Mater. 63 (2010) 905-908, http://dx.doi.org/10.1016/j.scriptamat.2010.06.040.

[26] Y.J. Liu, H.H. Yuan, H. Wang, Z.W. Wang. In Situ Transmission Electron Microscopy Investigation of Melting/Evaporation Kinetics in Anisotropic Gold Nanoparticles, Materials 14 (2021), http://dx.doi.org/10.3390/ma14237332.

[27] M. Wagih, C.A. Schuh. Spectrum of grain boundary segregation energies in a polycrystal, Acta Mater. 181 (2019) 228-237, http://dx.doi.org/10.1016/j.actamat.2019.09.034.

[28] N. Tuchinda, C. Li, C.A. Schuh. The Augmented Potential Method: Multiscale Modeling Toward a Spectral Defect Genome, (2025), http://dx.doi.org/10.48550/arXiv.2502.08014.

[29] P. Lejcek. On the anisotropy of grain-boundary segregation in multicomponent systems, Prog. Surf. Sci. 35 (1990) 209-213, http://dx.doi.org/10.1016/0079-6816(90)90045-L.

[30] S. Hofmann, P. Lejcek. Segregation at special grain boundaries in Fe-Si alloy bicrystals, J. Phys. Colloques 51 (1990) C1-179-C171-184, http://dx.doi.org/10.1051/jphyscol:1990127.

[31] H. Okamoto, T.B. Massalski. The Au−Pt (Gold-Platinum) system, Bulletin of Alloy Phase Diagrams 6 (1985) 46-56, http://dx.doi.org/10.1007/BF02871187.

[32] D. Wolf. Correlation between structure, energy, and ideal cleavage fracture for symmetrical grain-boundaries in fcc metals, J. Mater. Res. 5 (1990) 1708-1730, http://dx.doi.org/10.1557/JMR.1990.1708.

[33] K.C. Mills, Y.C. Su. Review of surface tension data for metallic elements and alloys: Part 1 - Pure metals, Int. Mater. Rev. 51 (2006) 329-351, http://dx.doi.org/10.1179/174328006X102510.

[34] D. McLean. Grain boundaries in metals, Clarendon Press, Oxford, 1957.

[35] J.M. Rickman, H.M. Chan, M.P. Harmer, J. Luo. Grain-boundary layering transitions in a model bicrystal, Surf. Sci. 618 (2013) 88-93, http://dx.doi.org/10.1016/j.susc.2013.09.004.

[36] P. Wynblatt, D. Chatain. Anisotropy of segregation at grain boundaries and surfaces, Metall. Mater. Trans. A 37A (2006) 2595-2620, http://dx.doi.org/10.1007/BF02586096.

[37] P. Wynblatt, D. Chatain. Solid-state wetting transitions at grain boundaries, Mater. Sci. Eng. A 495 (2008) 119-125, http://dx.doi.org/10.1016/j.msea.2007.09.091.

[38] N.X. Zhou, C.Z. Hu, J. Luo. Grain boundary segregation transitions and critical phenomena in binary regular solutions: A systematics of complexion diagrams with universal characters, Acta Mater. 221 (2021), http://dx.doi.org/10.1016/j.actamat.2021.117375.

[39] T.E. Hsieh, R.W. Balluffi. Observations of roughening de-faceting phase-transitions in grain boundaries, Acta Metall. 37 (1989) 2133-2139, http://dx.doi.org/10.1016/0001-6160(89)90138-7.

[40] M.N. Kelly, S.A. Bojarski, G.S. Rohrer. The temperature dependence of the relative grain-boundary energy of yttria-doped alumina, J. Am. Ceram. Soc. 100 (2017) 783-791, http://dx.doi.org/10.1111/jace.14488.

[41] B. Okkerse. Self-diffusion of gold, Phys. Rev. 103 (1956) 1246-1249, http://dx.doi.org/10.1103/PhysRev.103.1246.

[42] T.S. Lin, Y.W. Chung. Measurement of the activation-energy for surface-diffusion in gold by scanning tunneling microscopy, Surf. Sci. 207 (1989) 539-546, http://dx.doi.org/10.1016/0039-6028(89)90140-4.

[43] S.J. Dillon, M. Tang, W.C. Carter, M.P. Harmer. Complexion: A new concept for kinetic engineering in materials science, Acta Mater. 55 (2007) 6208-6218, http://dx.doi.org/10.1016/j.actamat.2007.07.029.